JACS
JOURNAL OF THE AMERICAN CHEMICAL SOCIETY
Article
pubs.acs.org/JACS

Fluoroketone Inhibition of Ca^{2+}-Independent Phospholipase A_2 through Binding Pocket Association Defined by Hydrogen/Deuterium Exchange and Molecular Dynamics

Yuan-Hao Hsu,*[,†,‡,⊥,▲] Denis Bucher,[‡,▲] Jian Cao,[†,‡] Sheng Li,[§] Sheng-Wei Yang,[⊥] George Kokotos,[▽] Virgil L. Woods, Jr,[§] J. Andrew McCammon,[†,‡,∥] and Edward A. Dennis*[,†,‡]

[†]Department of Pharmacology, [‡]Department of Chemistry and Biochemistry, [§]Department of Medicine, and [∥]Howard Hughes Medical Institute, University of California, San Diego, La Jolla, California 92093-0601, United States

[⊥]Department of Chemistry, Tunghai University, Taichung, Taiwan

[▽]University of Athens, Panepistimiopolis, Athens 15771, Greece

ABSTRACT: The mechanism of inhibition of group VIA Ca^{2+}-independent phospholipase A_2 ($iPLA_2$) by fluoroketone (FK) ligands is examined by a combination of deuterium exchange mass spectrometry (DXMS) and molecular dynamics (MD). Models for $iPLA_2$ were built by homology with the known structure of patatin and equilibrated by extensive MD simulations. Empty pockets were identified during the simulations and studied for their ability to accommodate FK inhibitors. Ligand docking techniques showed that the potent inhibitor 1,1,1,3-tetrafluoro-7-phenylheptan-2-one (PHFK) forms favorable interactions inside an active-site pocket, where it blocks the entrance of phospholipid substrates. The polar fluoroketone headgroup is stabilized by hydrogen bonds with residues Gly486, Gly487, and Ser519. The nonpolar aliphatic chain and aromatic group are stabilized by hydrophobic contacts with Met544, Val548, Phe549, Leu560, and Ala640. The binding mode is supported by DXMS experiments showing an important decrease of deuteration in the contact regions in the presence of the inhibitor. The discovery of the precise binding mode of FK ligands to the $iPLA_2$ should greatly improve our ability to design new inhibitors with higher potency and selectivity.

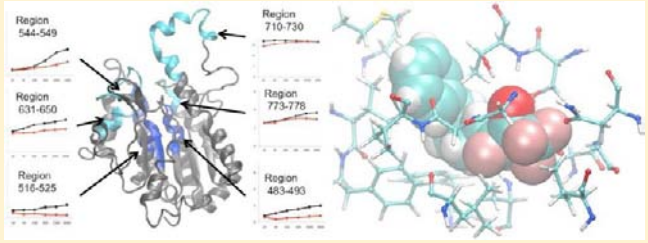

INTRODUCTION

Group VI phospholipase A_2 (GVI PLA_2), also known as Ca^{2+}-independent phospholipase A_2 ($iPLA_2$), constitutes one group of the superfamily of phospholipase A_2 enzymes that hydrolyzes the *sn*-2 ester bond of phospholipids to release free fatty acids.[1,2] These fatty acids can be metabolized into pro-inflammatory eicosanoids, including prostaglandins and leukotrienes.[3]

Ca^{2+}-independent phospholipases were so named after the discovery that their activity is not increased in the presence of Ca^{2+}, in contrast to the other then-known PLA_2s. The first discovered and best-studied $iPLA_2$ is the 85-kDa GVIA $iPLA_2$ (also known as $iPLA_2\beta$).[4] Different variants of $iPLA_2$s were later discovered, leading to their classification into various subgroups. To date, six subgroups have been identified, including GVIA ($iPLA_2\beta$; PNPLA9),[5−8] GVIB ($iPLA_2\gamma$; PNPLA8),[9,10] GVIC ($iPLA_2\delta$; PNPLA6),[11] GVID ($iPLA_2\varepsilon$; PNPLA3),[12] GVIE ($iPLA_2\xi$; PNPLA2),[13−15] and GVIF PLA_2 ($iPLA_2\eta$; PNPLA4).[2,16−18] These GVI $iPLA_2$s all contain a serine active site in a patatin-like catalytic domain. GVIA $iPLA_2$ has been reported to be activated by oligomerization, ATP binding, caspase cleavage, and membrane interaction[1] and to localize in mitochondria in various types of cells.[19−21]

The important roles of $iPLA_2$ in regulation of the inflammatory response and in mitochondrial maintenance suggest that it could be implicated in a large number of genetic and age-related diseases. GVIA $iPLA_2$ has been suggested to be responsible for the deacylation of cardiolipin and monolysocardiolipin accumulation in Barth syndrome and hypertensive heart failure.[22,23] Clinical studies have demonstrated that mutations of GVIA $iPLA_2$ are associated with "neurodegeneration with brain iron accumulation" (NBIA) disorders and infantile neuroaxonal dystrophy.[24−27] Recently, it was demonstrated that GVIA $iPLA_2$ plays a key role in the onset and progression of experimental autoimmune encephalomyelitis (EAE) indicating that this enzyme may be a target for the development of novel therapies for multiple sclerosis.[28] Recent cellular studies have also suggested that $iPLA_2$ may interfere with the protein p53 pathway. In particular, inhibition of $iPLA_2$ was shown to decrease prostate cancer cell growth, suggesting $iPLA_2$ could be a new anticancer target.[29,30]

Due to the considerable pharmaceutical interest in $iPLA_2$, a current challenge is the design of a safe inhibitor that is also highly selective for this class. Several ligands have already been shown to inhibit the phospholipase, lysophospholipase, and transacylase activities of GVIA $iPLA_2$.[31−34] The most commonly used $iPLA_2$ inhibitor is bromoenol lactone (BEL),

Received: July 3, 2012
Published: December 20, 2012

   dx.doi.org/10.1021/ja306490g | *J. Am. Chem. Soc.* 2013, 135, 1330−1337

and the *S* enantiomer (*S*-BEL), has been shown to preferentially inhibit $iPLA_2$.[33−37] Although BEL inhibits $iPLA_2$ through acylation of a critical cysteine,[38] it is also highly toxic, as it reacts with cysteines in other proteins. Methyl arachidonyl fluorophosphonates, known as MAFP, are potent inhibitors of $iPLA_2$[31] but their action is irreversible, which typically translates into increased toxicity in vivo. In addition, 2-oxoamides have been shown to inhibit GVIA $iPLA_2$ but are also active against GIVA $cPLA_2$.[39] Finally, fatty acyl trifluoromethyl ketones, including arachidonyl and palmitoyl trifluoromethyl ketones, have been identified as promising inhibitors of GVIA $iPLA_2$.[33] Fluoroketone (FK) inhibitors were designed to target serine active sites and consequently are also active against $cPLA_2$. However, FK inhibitors were shown to become selective for $iPLA_2$ versus $cPLA_2$ and $sPLA_2$, after a modification of the fluoroketone group, and the addition of a hydrophobic terminus connected by a medium-length carbon chain to mimic the fatty acid chain.[40] One pentafluoroketone, FKGK11, has been shown to be a potent and selective GVIA $iPLA_2$ inhibitor demonstrating in vivo activity against EAE.[27] Another FK ligand, 1,1,1,3-tetrafluoro-7-phenylheptan-2-one (PHFK),[40] contains a phenyl ring, a five-carbon linker, and an additional fluorine on the carbon adjacent to the ketone of the trifluoromethylketone. It shows great promise as a lead compound for $iPLA_2$-associated diseases; hence, we have focused in this paper on resolving its binding mode.

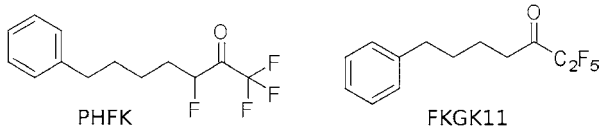

Previous computational studies on the inhibition of PLA_2 have mainly focused on group IVA (GIVA, $cPLA_2$) proteins,[41,42] where high-resolution structural data exist. The task of determining the binding mode of FK inhibitors for GVIA PLA_2 is complicated by the lack of high-resolution X-ray structures. GVI $iPLA_2$ enzymes are known to be composed of an N-terminal regulatory domain containing seven ankyrin repeats and a C-terminal catalytic domain containing the active-site dyad (Ser519/Asp652) (Figure 1A). The catalytic domain has low sequence homology to other lipases, such as $cPLA_2$, and is distinct from the highly disulfide-bonded $sPLA_2$s. Previously, we proposed a rudimentary model of the catalytic domain based on the structure of the patatin protein,[43] a lipid acyl hydrolase found in potato with sequence similarity with the catalytic domain of $iPLA_2$. The model could explain why some regions of the catalytic domain appeared particularly accessible to the solvent in deuterium exchange mass spectrometry (DXMS) experiments.[43] However, the binding of inhibitors and the stability of the model in molecular dynamics (MD) simulations were not studied.

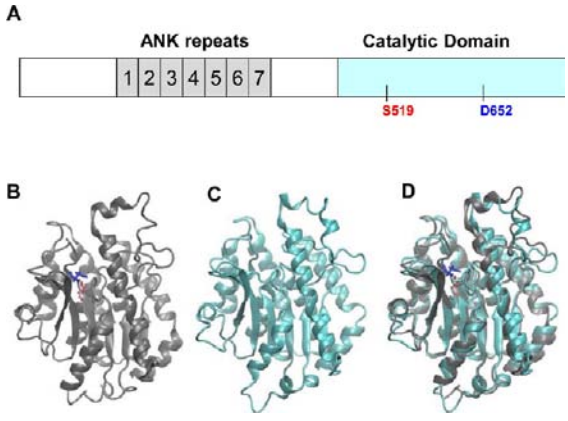

Figure 1. (A) Schematic representation of GVIA $iPLA_2$ sequence information with the location of the active-site dyad, Ser519/Asp652. (B) Initial guess for the structure of the catalytic domain based on patatin. (C) Equilibrated structure after extensive (∼200 ns) MD simulation. (D) Superposition between initial guessed structure and equilibrated structure, showing a high degree of consistency.

In this paper, computational methods are coupled with experimental DXMS techniques to study the atomic-level details of the $iPLA_2$−PHFK complex. A new model for the catalytic domain of $iPLA_2$ is proposed and shown to be stable by extensive MD simulations under aqueous conditions. Ligand docking techniques were able to uncover a favorable binding mode for FK inhibitors, and H/D exchange experiments provide experimental information about the effect of PHFK binding on solvent accessibility, giving strong support to the proposed binding mode. The details of protein−inhibitor interactions are discussed, as well as implications for the catalytic mechanism.

MATERIALS AND METHODS

Materials. 1-Palmitoyl-2-arachidonoyl-*sn*-phosphatidylcholine (PAPC) was obtained from Avanti Polar Lipids, and D_2O (99.96%) was obtained from Cambridge Isotope Laboratories. The PHFK ligand was synthesized as previously described.[40] All other reagents were analytical reagent grade or better.

Protein Expression, Purification, and Activity Assay. GVIA $iPLA_2$ containing an N-terminal His_6-tagged insertion at the third residue was expressed by use of recombinant baculovirus in suspension cultures of Sf9 insect cells.[43] For the specific activity of $iPLA_2$, assays (Figure 3) were performed in buffer composed of 100 mM *N*-(2-hydroxyethyl)piperazine-*N*′-ethanesulfonic acid (HEPES) at pH 7.5, 2 mM ATP, and 5 mM dithiothreitol (DTT). The mixed micelles were composed of 0.1 mM PAPC (80 000 cpm) and 0.4 mM Triton X-100 in a final volume of 500 μL. The reaction was initiated by adding 0.2 μg of $iPLA_2$ to mixed micelles and incubated at 40 °C for 30 min. After incubation, the reaction was quenched, and the fatty acids were extracted by a modified Dole protocol as previously described.[40]

Preparation of Deuterated Samples. Before the DXMS experiments were carried out, 5 mM PHFK inhibitor (100× stock in 100% dimethyl sulfoxide, DMSO) was added to $iPLA_2$ to a final 50 μM PHFK in 1% DMSO and incubated at 23 °C for 10 min. Control experiments contain 1% DMSO. Hydrogen/deuterium exchange experiments were initiated by mixing 40 μL of $iPLA_2$ (containing 50 μg of $iPLA_2$) in protein buffer with 80 μL of D_2O buffer to a final concentration of 63.3% D_2O at pH 7.0. D_2O buffer was prepared by mixing 99.99% D_2O with 20× buffer solution in H_2O and generated 95% D_2O buffer. Final D_2O buffer contained 50 mM 3-(*N*-morpholino)propanesulfonic acid (MOPS) (pH 6.9), 100 mM NaCl, 2 mM DTT, and 2 mM ATP.

The samples were incubated at 23 °C for an additional 10, 30, 100, 300, 1000, or 3000 s. The deuterium exchange was quenched by adding 80 μL of ice-cold quench solution (2.5% formic acid, 2.5 M guanidine hydrochloride) that acidified the sample to a final pH = 2.5. The samples were then immediately frozen on dry ice. Back exchange levels were calculated as previously reported.[43,44] Vials with frozen samples were stored at −80 °C until analysis, usually within 3 days.

Proteolysis−Liquid Chromatography−Mass Spectrometry Analysis of Samples. All steps were performed at 0 °C as previously described.[43−45] The quenched sample was digested by porcine pepsin-immobilized column and the proteolyzed peptides were separated on a C18 column.The peptides were analyzed on an LCQ Classic (Thermo Finnigan, Inc.) electrospray ion trap-type mass spectrometer and an

dx.doi.org/10.1021/ja306490g | *J. Am. Chem. Soc.* 2013, 135, 1330−1337

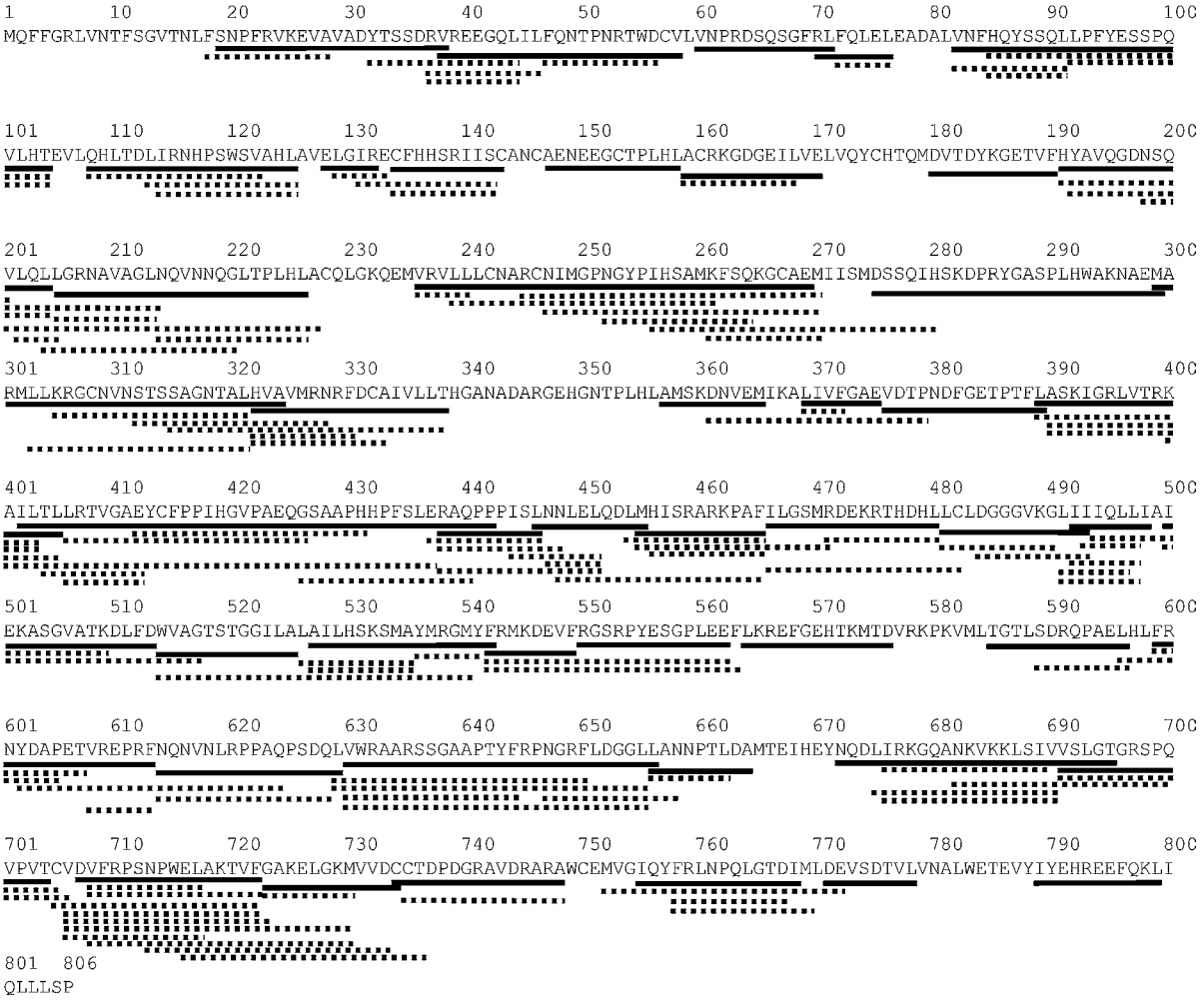

Figure 2. Pepsin-digested peptide coverage map of GVIA iPLA$_2$. Peptides shown as solid lines were used to depict the deuteration level by use of the color index in Figure 4.

electrospray Q-TOF (time-of-flight) mass spectrometer (Micromass). Peptides were identified by tandem mass spectrometry (MS/MS) data through SEQUEST (Thermo Finnigan, Inc.). DXMS Explorer (Sierra Analytics Inc., Modesto CA) was used to analyze the mass spectra and calculate the average of the mass envelope. The procedure for further data processing was described previously.[43,44]

iPLA$_2$ Coverage Map of Pepsin Fragmentation and Deuterium On-Exchange. The recombinant iPLA$_2$ after purification was confirmed to be active in the mixed-micelle assay. The procedure of protein digestion by pepsin was previously described.[43] Among them, 153 peptides had a sufficient signal-to-noise ratio for analysis, which covered 88% of the total protein sequence. From these 110 peptides, 46 different peptides with the least number of overlapped residues were selected to determine the deuteration level of iPLA$_2$ (Figure 2). Overall, the representative 46 peptides selected account for 71% coverage of the iPLA$_2$.

Deuterium exchange experiments were carried out by incubation of 40 μL of iPLA$_2$ with 80 μL of 95% D_2O buffer for six different time points (10, 30, 100, 300, 1000, and 3000 s) at 23 °C. The sample was quenched and injected onto the HPLC online digestion system.[43−45] The triplicate experiments were carried out with three different batches of enzyme on different days. The deuteration level increase over time due to the amide H/D exchange. The exchange results in various regions were calculated as the ratio of incorporated deuterons to the maximum deuteration in a particular peptide (Figure 4). Because of the fast off-exchange rate of N-terminal residues, these residues are unable to retain any deuterons under the experimental conditions employed; hence, these residues were not shown in the results. Some peptides that showed a poor signal-to-noise ratio after deuteration were also excluded from analysis.

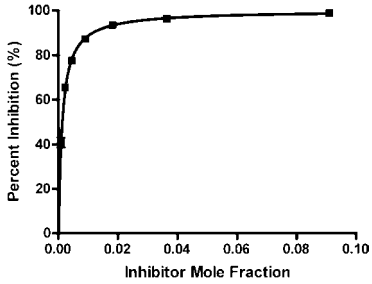

Figure 3. Inhibition of the activity of human GVIA iPLA$_2$ by PHFK [$X_I(50)$ = 0.0013] tested on mixed micelles.

Structural Models and MD Simulation. The Prime protein structure prediction suite[46] was used to build a homology model for the catalytic domain of iPLA$_2$, using as a template the X-ray structure of patatin (40% sequence homology), solved at a resolution of 2.2 Å (PDB code 1OXW).[47] The 329 amino acid model for the catalytic domain was solvated in VMD,[48] in a cubic periodic box containing a physiological concentration of Na^+ and Cl^- ions of 0.10 mol/L. Ionizable side chains were kept in their default charge states for pH 7, and the His residues were kept uncharged. All simulations were conducted in NAMD 2.9[49] with the CHARMM27 force field.[50] A time step of 2.0 fs was used in combination with the SHAKE algorithm.[51] The temperature was regulated with a Langevin thermostat.[52]

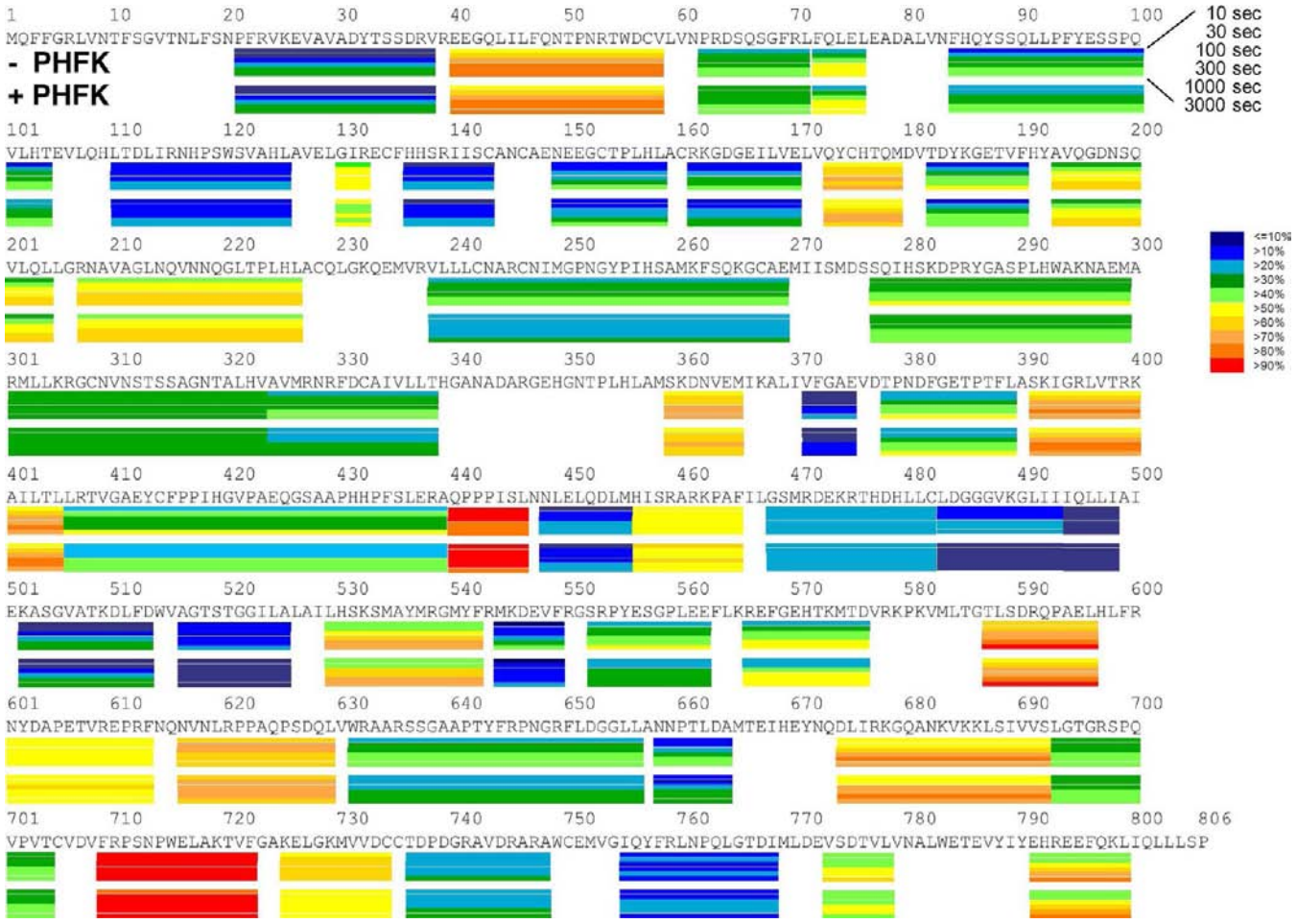

Figure 4. Deuterium exchange of GVIA iPLA$_2$ with and without PHFK inhibitor. Each bar under the primary sequence is divided into rows corresponding to different time points from 10 s to 50 min (top to bottom). The color coding indicates the percent of H/D exchange during the given time period.

Energy minimization was conducted for 25 000 steps with the protein backbone atoms fixed, followed by two consecutive 20 ns MD runs in the NPT and NVT ensembles. Subsequently, two production runs were conducted for 200 ns in the NVT ensemble. The overall structural stability of the model was indicated by a stable root-mean-square-deviation (RMSD) for the backbone atom positions during the simulations. After only ~3 ns of MD, the potential energy had reached a plateau and the RMSD of backbone atoms stabilized below 3 Å. Inspection of the trajectories revealed that the integrity of the secondary structure was maintained (Figure 1C). In the spirit of the relaxed complex scheme,[53] trajectories were clustered into a reduced ensemble of 50 representative structures for ligand docking. Empty pockets inside the protein were monitored by computing the solvent-accessible surface in VMD. The ligand was docked with Glide software,[54] using the OPLS-2005 force field for its parametrization[55] and an inner docking box of length 10 Å.

RESULTS AND DISCUSSION

DXMS Characterization of iPLA$_2$–PHFK Interaction. The significant deuteration changes upon PHFK binding are located in the catalytic domain of iPLA$_2$ (Figure 5). In particular, five regions surrounding the active-site dyad, residues 483–493, 516–525, 544–549, 631–655, and 773–778, showed the most significant decrease of deuteration (Figure 6), while none of the regions showed an increase in H/D exchange.

Region 483–493 contains the DXMS information from three peptide fragments: 483–490, 483–493, and 486–493. In the absence of inhibitor, the deuteration level was observed to increase, from 10% to 30%, from 10 s to 50 min. The same experiment repeated in the presence of PHFK led to a deuteration level below 10% during the whole 50 min time course. Region 493–498 is located in a stable helix next to the C-terminus of region 483–493. It showed a very slow H/D exchange, of only 2%, after 50 min. Region 516–525, which contains the active-site Ser519, showed a clear decrease in deuteration upon PHFK binding. The largest decrease in this region was 18% at 50 min of exchange. Similarly, region 544–549 showed a significant decrease of deuteration after 16 min of H/D exchange. Region 631–655 contains fragments 631–650, 631–655, 632–655, and 632–656 from four individual peptides. Among these regions, the 631–650 fragment seems to be responsible for most of the changes. Region 773–778 showed a 12% decrease of H/D exchange at the 50 min time point, and region 710–730 showed 12% and 9% decrease of exchange after 10 and 30 s, respectively. Regions 404–442 in the linker region and 238–269 in the ankyrin repeats also showed greater than 10% decrease in H/D exchange.

Computational Characterization of the iPLA$_2$–PHFK Interaction. MD simulations showed that iPLA$_2$ residues, including active-site residues, are flexible (RMS fluctuation = ~0.6–0.8 Å). An analysis of the solvent-accessible surface

dx.doi.org/10.1021/ja306490g | J. Am. Chem. Soc. 2013, 135, 1330–1337

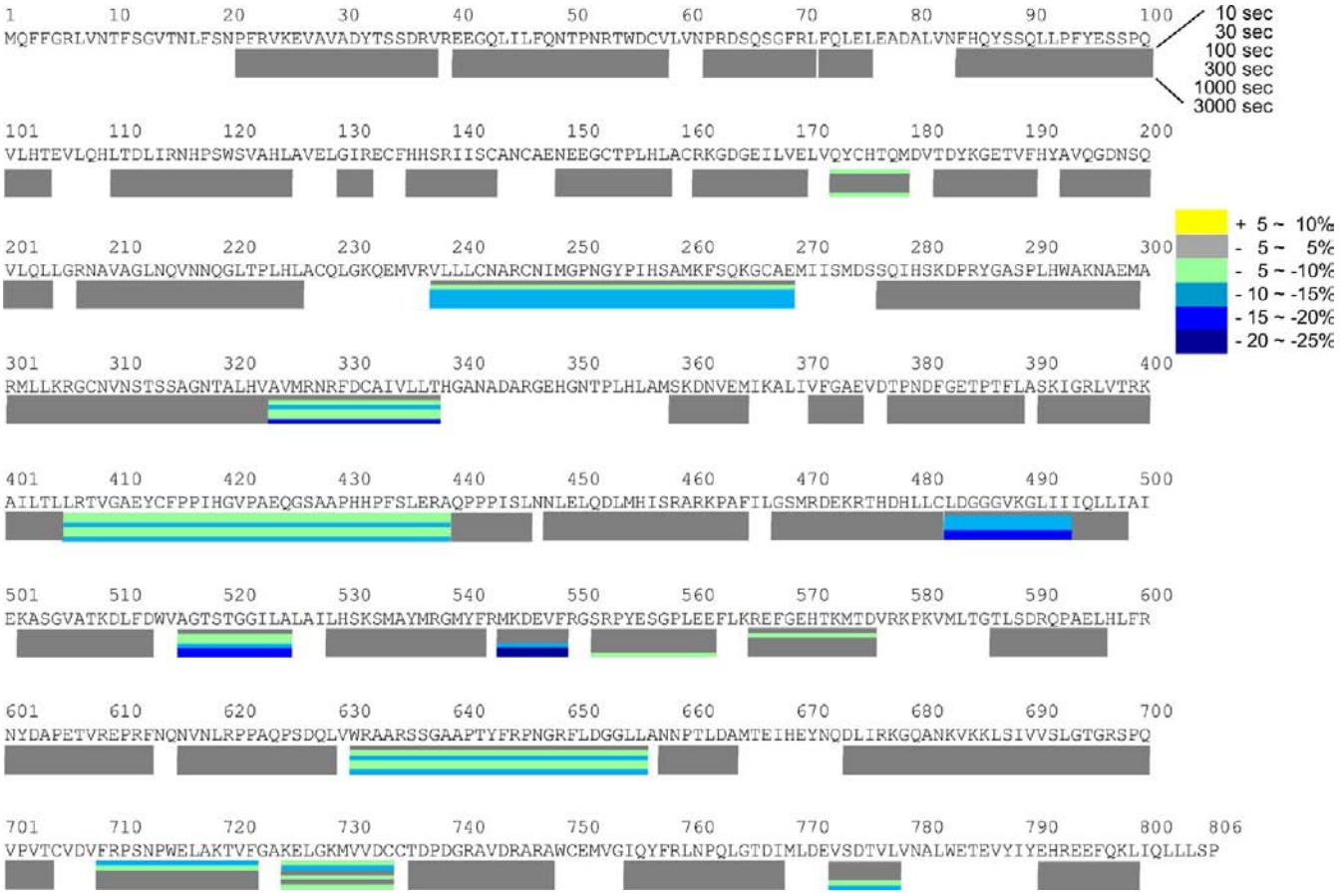

Figure 5. Effect of PHFK binding on H/D exchange levels in iPLA$_2$ for six time points from 10 s to 50 min. The color coding indicates the deuteration level changes during the time period.

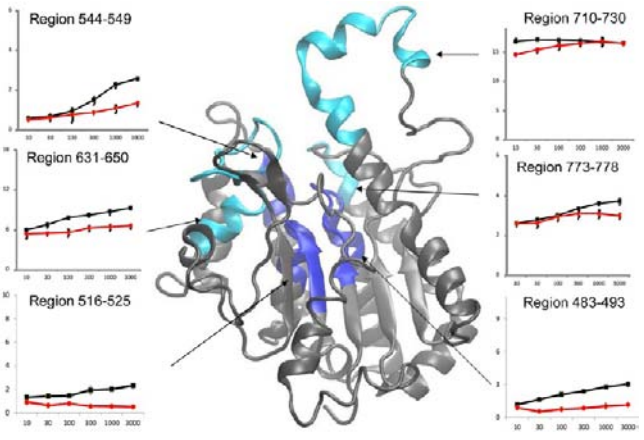

Figure 6. Regions of H/D exchange most affected by PHFK binding. The deuteron number is shown for each fragment in the presence (black squares) and absence (red circles) of inhibitor. The black and red curves indicate the number of H/D exchanges at six time points corresponding to 10, 30, 100, 300, 1000, and 3000 s. Color coding of structure is as shown in Figure 5.

during 2 × 200 ns MD simulations was carried out to discover transient pockets that could potentially accommodate the PHFK inhibitor. Fifty representative protein structures were extracted from the simulations. An analysis of the solvent accessibility surface revealed that several empty pockets were large enough to accommodate the inhibitor, including an empty pocket near the active-site Ser519. Ligand docking was performed on all the pockets and indicated that the best docking scores were systematically obtained when the box was centered on the active site, suggesting a very favorable binding mode.

In Figure 7, the docked iPLA$_2$−PHFK complex is shown. The inhibitor is found to sit snugly in the active-site with its FK group stabilized by polar residues, and its alkyl chain and benzene ring stabilized by nonpolar side-chains (Figure 8). More specifically, the carbonyl group of PHFK forms favorable interactions with the amide groups of Gly486 and Gly487. A "fluorophilic site" is created by Lys489, Asn658, and Lys729, while the aliphatic carbon chain is stabilized by a narrow hydrophobic tunnel formed by residues Thr520, Phe549, and Leu770. The benzene ring forms hydrophobic contacts with Met544, Val548, Phe549, and Leu560. DXMS experiments indicate that these residues display decreased H/D exchange in the presence of the PHFK ligand (Table 1), in agreement with the proposed binding mode. Such a noncovalent binding model is in accordance with previous results demonstrating reversible inhibition of iPLA$_2$ by trifluoromethyl ketones.[56] Various experimental results demonstrated that the mechanism of inhibition of iPLA$_2$ by FKs is quite different than that observed by cPLA$_2$. In the case of iPLA$_2$, the reaction progress curve was linear and the binding was fast, indicating a reversible inhibition not involving slow or tight binding.[56]

Regulation and Flexibility of iPLA$_2$. The complete structure of iPLA$_2$ includes seven ankyrin repeats, a linker, and a catalytic domain. The ankyrin repeats are connected to

dx.doi.org/10.1021/ja306490g | J. Am. Chem. Soc. 2013, 135, 1330−1337

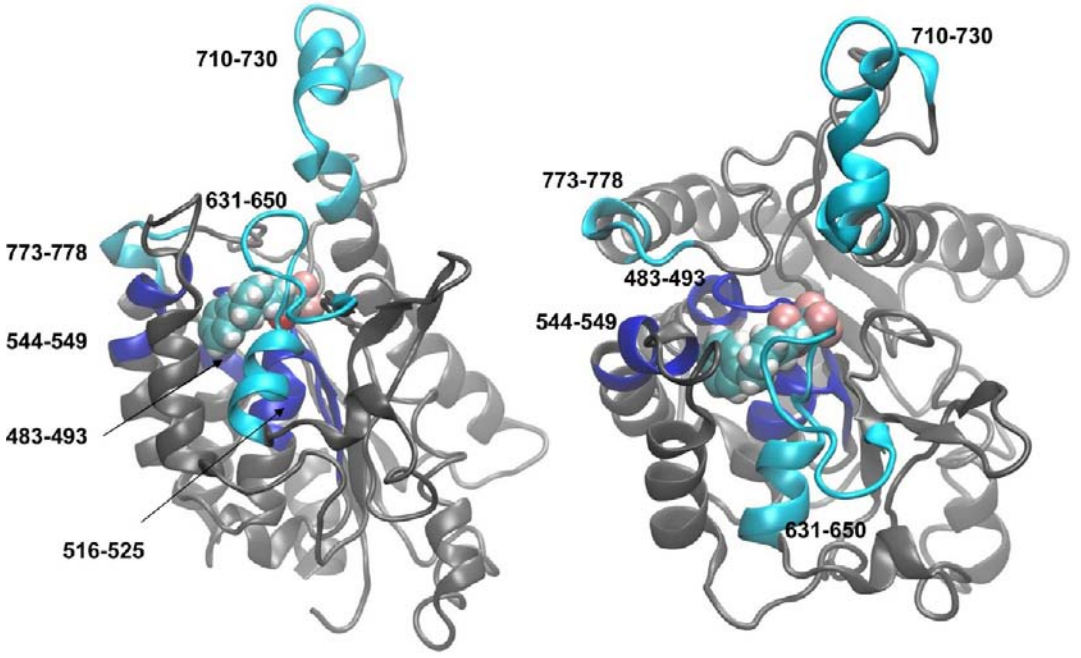

Figure 7. Location of PHFK binding to $iPLA_2$ according to ligand docking and DXMS experiments. The color code indicates regions of decreased H/D exchange upon ligand binding. The membrane penetration domain (loop 695−730) is believed to anchor the protein at the membrane surface by entering the membrane. The left and right images correspond to the protein viewed from a direction parallel or perpendicular to the membrane surface.

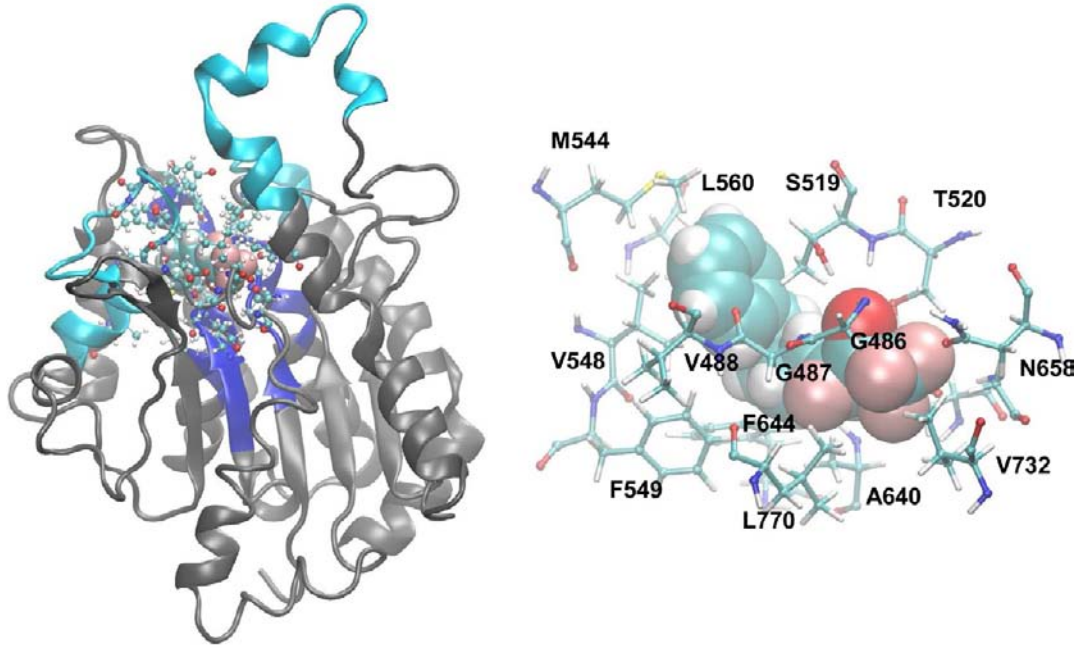

Figure 8. Characterization of the inhibitor binding pocket in the catalytic domain of $iPLA_2$. Residues within a 5 Å radius of PHFK are shown.

the catalytic domain through the linker. Whether and how ankyrin repeats regulate the catalytic activity of $iPLA_2$ remains unclear. DXMS experiments suggest that inhibitor binding to $iPLA_2$ decreases the rates of H/D exchange, with most changes appearing in the loops surrounding the active site in the catalytic domain. The decrease in H/D exchange in these regions appears to be fully explained by direct contact with the inhibitor, blocking access to phospholipid substrates and reducing solvent accessibility. However, a minor decrease in H/D exchange was also observed in the linker region and the ankyrin repeats, indicating that the perturbation caused by inhibitor can extend to the whole enzyme. Because only one linker region and one ankyrin region showed a small 10% decrease of deuteration after 30 min of H/D exchange, overall, the structure of the ankyrin repeats and the linker is unlikely to change dramatically, and only minor shifts in the relative positions between the ankyrin repeats and the catalytic domain may occur upon ligand binding. One cannot exclude that phospholipid substrates may have different properties when compared to the PHFK inhibitor studied here; however, we

dx.doi.org/10.1021/ja306490g | J. Am. Chem. Soc. 2013, 135, 1330−1337

Table 1. DXMS Character of Residues in the Inhibitor Binding Pocket

	DXMS (50 min), %			
	$iPLA_2$	$iPLA_2$–PHFK	DXMS change, %	secondary structure
Gly485	35	12	23	loop
Gly486	35	12	23	loop
Gly487	35	12	23	loop
Lys489	35	12	23	loop
Thr518	23	5	18	loop
Ser519	23	5	18	loop
Thr520	23	5	18	helix
Gly521	23	5	18	helix
Ile523	23	5	18	helix
Met544	42	21	21	helix
Lys545	42	21	21	helix
Val548	42	21	21	helix
Phe549	42	21	21	helix
Leu560	56	47	8	helix
Ala640	51	36	15	loop
Tyr643	51	36	15	loop
Phe644	51	36	15	loop
Asn658	44	40	4	loop
Val732	64	59	6	helix

expect the perturbation caused by ligand binding to remain localized to the active site in both cases.

The active-site dyad, Ser519 and Asp652, is conserved in both patatin and $iPLA_2$. Asp652 is believed to accept a hydrogen from Ser519 during the initial stages of the catalytic reaction. Interestingly, no hydrogen bond is present between the two residues in the crystal structure of patatin, which shows instead a separation of 3.7 Å. Both Ser519 and Asp652 are strongly affected by PHFK binding. Ser519 is located in the region 516–525, showing a H/D exchange decrease of 18%, and Asp652 is in the region 632–655, which shows a decrease of 11%. MD simulations of the protein–PHFK complex suggests that the binding of PHFK helps shorten the distance between Ser519 H and Asp652 O, from 3.7 to 1.6 Å, creating a hydrogen bond between the two residues. This hydrogen bond was also observed in MD simulations of the apoprotein, where it was seen to typically break and re-form within ~1 ns.

The regulation of active-site accessibility by the surrounding flexible loops is another interesting possibility. The structure of the catalytic domain of $iPLA_2$ is similar to the core structure of $cPLA_2$, which is one of the well-studied PLA_2s. Unlike the buried active sites of $cPLA_2$, $iPLA_2$ has a more exposed catalytic domain. However, the active-site serine is surrounded by several flexible loops that could provide some form of regulation, including residues 485–487 (glycine loop), 517–520 (catalytic loop), 540–545, 549–560, 631–653, 695–730 (membrane penetration arm), and 761–775. MD simulations confirmed a high degree of flexibility in the loop regions, in particular in the membrane penetration arm domains, (loop 695–730), which could play a role similar to the cap structure of $cPLA_2$. DXMS experiments show that the effect of PHFK binding propagates to the loop regions, suggesting some degree of conformational flexibility in the unstructured loops. In particular, regions 710–722 and 710–730 in the membrane penetration arm showed a very slight drop of 7% and 12% in the deuteration level at 10 s of H/D exchange. This domain was previously found to undergo a dramatic decrease of H/D exchange upon binding to membranes.[43] However, it appears to be only slightly affected by inhibitor binding, with a small degree of change relative to residues in direct contact with the inhibitor. Thus, we do not expect the binding of PHFK to lead to complete collapse of the membrane penetration arm to cover the active site, although the loop could still help create some form of regulation.

CONCLUDING REMARKS

Ligands containing a trifluoromethyl or pentafluoroethyl ketone and a hydrophobic tail have been identified as potent and selective inhibitors of GVIA $iPLA_2$,[40] encouraging their utility in developing new pharmaceutical agents. Computer modeling and DXMS experiments show that the binding of FK ligands occurs in the active site, with the inhibitors mimicking the binding of natural substrates. In the natural enzyme, hydrophobic interactions with the phospholipid tail are believed to help increase the binding affinity of the reactant with respect to the lysophospholipid product. Similarly, in the $iPLA_2$–PHFK complex, favorable hydrophobic interactions can explain the high affinity of the inhibitor. In addition, the perfluoroalkyl headgroup of FK ligands can substitute for the headgroup of the phospholipids and enter a fluorophilic site, while the oxyanion hole in the triglycine region is able to stabilize the FK carbonyl group through strong hydrogen bonds. The abundant empty space on both sides of the docked PHFK inhibitor suggests why FK ligands with larger head or tail groups are also able to bind to $iPLA_2$.[40] Discovery of the binding mode for PHFK and the available space for further decoration of the primary inhibitor represents an important first step toward the rational design of new selective inhibitors. In future work, chemical alterations of current inhibitors will be pursued, based on the binding mode and structural model presented here.

AUTHOR INFORMATION

Corresponding Author

edennis@ucsd.edu; howardhsu@thu.edu.tw

Author Contributions

▲These authors contributed equally.

Notes

The authors declare no competing financial interest.

ACKNOWLEDGMENTS

We thank Dr. Varnavas D. Mouchlis for critically reviewing the manuscript and for helpful suggestions. This work was supported by NIH Grants RO1-GM20501 (E.A.D), GM093325 and RR029388 (V.L.W.), and the San Diego Super Computer Center (SDSC). D.B. and J.A.M. were supported in part by NSF, NIH, HHMI, NBCR, and CTBP.

REFERENCES

(1) Dennis, E. A.; Cao, J.; Hsu, Y. H.; Magrioti, V.; Kokotos, G. *Chem. Rev.* **2011**, *111*, 6130.
(2) Six, D. A.; Dennis, E. A. *Biochim. Biophys. Acta* **2000**, *1488*, 1.
(3) Buczynski, M. W.; Dumlao, D. S.; Dennis, E. A. *J. Lipid Res.* **2009**, *50*, 1015.
(4) Ackermann, E. J.; Kempner, E. S.; Dennis, E. A. *J. Biol. Chem.* **1994**, *269*, 9227.
(5) Balboa, M. A.; Balsinde, J.; Jones, S. S.; Dennis, E. A. *J. Biol. Chem.* **1997**, *272*, 8576.
(6) Sedgwick, S. G.; Smerdon, S. J. *Trends Biochem. Sci.* **1999**, *24*, 311.

(7) Tang, J.; Kriz, R. W.; Wolfman, N.; Shaffer, M.; Seehra, J.; Jones, S. S. *J. Biol. Chem.* **1997**, *272*, 8567.
(8) Wolf, M. J.; Gross, R. W. *J. Biol. Chem.* **1996**, *271*, 30879.
(9) Mancuso, D. J.; Jenkins, C. M.; Gross, R. W. *J. Biol. Chem.* **2000**, *275*, 9937.
(10) Tanaka, H.; Takeya, R.; Sumimoto, H. *Biochem. Biophys. Res. Commun.* **2000**, *272*, 320.
(11) van Tienhoven, M.; Atkins, J.; Li, Y.; Glynn, P. *J. Biol. Chem.* **2002**, *277*, 20942.
(12) Baulande, S.; Lasnier, F.; Lucas, M.; Pairault, J. *J. Biol. Chem.* **2001**, *276*, 33336.
(13) Jenkins, C. M.; Mancuso, D. J.; Yan, W.; Sims, H. F.; Gibson, B.; Gross, R. W. *J. Biol. Chem.* **2004**, *279*, 48968.
(14) Villena, J. A.; Roy, S.; Sarkadi-Nagy, E.; Kim, K. H.; Sul, H. S. *J. Biol. Chem.* **2004**, *279*, 47066.
(15) Zimmermann, R.; Strauss, J. G.; Haemmerle, G.; Schoiswohl, G.; Birner-Gruenberger, R.; Riederer, M.; Lass, A.; Neuberger, G.; Eisenhaber, F.; Hermetter, A.; Zechner, R. *Science* **2004**, *306*, 1383.
(16) Lee, W. C.; Salido, E.; Yen, P. H. *Genomics* **1994**, *22*, 372.
(17) Kienesberger, P. C.; Oberer, M.; Lass, A.; Zechner, R. *J. Lipid Res.* **2009**, *50* (Suppl.), S63.
(18) Saarela, J.; Jung, G.; Hermann, M.; Nimpf, J.; Schneider, W. J. *BMC Genomics* **2008**, *9*, 281.
(19) Gadd, M. E.; Broekemeier, K. M.; Crouser, E. D.; Kumar, J.; Graff, G.; Pfeiffer, D. R. *J. Biol. Chem.* **2006**, *281*, 6931.
(20) Liou, J. Y.; Aleksic, N.; Chen, S. F.; Han, T. J.; Shyue, S. K.; Wu, K. K. *Exp. Cell Res.* **2005**, *306*, 75.
(21) Seleznev, K.; Zhao, C.; Zhang, X. H.; Song, K.; Ma, Z. A. *J. Biol. Chem.* **2006**, *281*, 22275.
(22) Malhotra, A.; Edelman-Novemsky, I.; Xu, Y.; Plesken, H.; Ma, J.; Schlame, M.; Ren, M. *Proc. Natl. Acad. Sci. U.S.A.* **2009**, *106*, 2337.
(23) Zachman, D. K.; Chicco, A. J.; McCune, S. A.; Murphy, R. C.; Moore, R. L.; Sparagna, G. C. *J. Lipid Res.* **2010**, *51*, 525.
(24) Gregory, A.; Westaway, S. K.; Holm, I. E.; Kotzbauer, P. T.; Hogarth, P.; Sonek, S.; Coryell, J. C.; Nguyen, T. M.; Nardocci, N.; Zorzi, G.; Rodriguez, D.; Desguerre, I.; Bertini, E.; Simonati, A.; Levinson, B.; Dias, C.; Barbot, C.; Carrilho, I.; Santos, M.; Malik, I.; Gitschier, J.; Hayflick, S. J. *Neurology* **2008**, *71*, 1402.
(25) Tonelli, A.; Romaniello, R.; Grasso, R.; Cavallini, A.; Righini, A.; Bresolin, N.; Borgatti, R.; Bassi, M. T. *Clin. Genet.* **2010**, *78*, 432.
(26) Kurian, M. A.; Morgan, N. V.; MacPherson, L.; Foster, K.; Peake, D.; Gupta, R.; Philip, S. G.; Hendriksz, C.; Morton, J. E.; Kingston, H. M.; Rosser, E. M.; Wassmer, E.; Gissen, P.; Maher, E. R. *Neurology* **2008**, *70*, 1623.
(27) Morgan, N. V.; Westaway, S. K.; Morton, J. E.; Gregory, A.; Gissen, P.; Sonek, S.; Cangul, H.; Coryell, J.; Canham, N.; Nardocci, N.; Zorzi, G.; Pasha, S.; Rodriguez, D.; Desguerre, I.; Mubaidin, A.; Bertini, E.; Trembath, R. C.; Simonati, A.; Schanen, C.; Johnson, C. A.; Levinson, B.; Woods, C. G.; Wilmot, B.; Kramer, P.; Gitschier, J.; Maher, E. R.; Hayflick, S. J. *Nat. Genet.* **2006**, *38*, 752.
(28) Kalyvas, A.; Baskakis, C.; Magrioti, V.; Constantinou-Kokotou, V.; Stephens, D.; Lopez-Vales, R.; Lu, J. Q.; Yong, V. W.; Dennis, E. A.; Kokotos, G.; David, S. *Brain* **2009**, *132*, 1221.
(29) Sun, B.; Zhang, X.; Yonz, C.; Cummings, B. S. *Biochem. Pharmacol.* **2010**, *79*, 1727.
(30) Sun, B.; Zhang, X.; Talathi, S.; Cummings, B. S. *J. Pharmacol. Exp. Ther.* **2008**, *326*, 59.
(31) Lio, Y. C.; Reynolds, L. J.; Balsinde, J.; Dennis, E. A. *Biochim. Biophys. Acta* **1996**, *1302*, 55.
(32) Lio, Y. C.; Dennis, E. A. *Biochim. Biophys. Acta* **1998**, *1392*, 320.
(33) Ackermann, E. J.; Conde-Frieboes, K.; Dennis, E. A. *J. Biol. Chem.* **1995**, *270*, 445.
(34) Hazen, S. L.; Zupan, L. A.; Weiss, R. H.; Getman, D. P.; Gross, R. W. *J. Biol. Chem.* **1991**, *266*, 7227.
(35) Magrioti, V.; Kokotos, G. *Expert Opin. Ther. Pat.* **2010**, *20*, 1.
(36) Balsinde, J.; Bianco, I. D.; Ackermann, E. J.; Conde-Frieboes, K.; Dennis, E. A. *Proc. Natl. Acad. Sci. U.S.A.* **1995**, *92*, 8527.
(37) Jenkins, C. M.; Han, X.; Mancuso, D. J.; Gross, R. W. *J. Biol. Chem.* **2002**, *277*, 32807.
(38) Song, H.; Ramanadham, S.; Bao, S.; Hsu, F. F.; Turk, J. *Biochemistry* **2006**, *45*, 1061.
(39) Barbayianni, E.; Stephens, D.; Grkovich, A.; Magrioti, V.; Hsu, Y. H.; Dolatzas, P.; Kalogiannidis, D.; Dennis, E. A.; Kokotos, G. *Bioorg. Med. Chem.* **2009**, *17*, 4833.
(40) Kokotos, G.; Hsu, Y. H.; Burke, J. E.; Baskakis, C.; Kokotos, C. G.; Magrioti, V.; Dennis, E. A. *J. Med. Chem.* **2010**, *53*, 3602.
(41) Burke, J. E.; Babakhani, A.; Gorfe, A. A.; Kokotos, G.; Li, S.; Woods, V. L., Jr.; McCammon, J. A.; Dennis, E. A. *J. Am. Chem. Soc.* **2009**, *131*, 8083.
(42) Mouchlis, V. D.; Michopoulou, V.; Constantinou-Kokotou, V.; Mavromoustakos, T.; Dennis, E. A.; Kokotos, G. *J. Chem. Inf. Model.* **2012**, *52*, 243.
(43) Hsu, Y. H.; Burke, J. E.; Li, S.; Woods, V. L., Jr.; Dennis, E. A. *J. Biol. Chem.* **2009**, *284*, 23652.
(44) Hsu, Y. H.; Burke, J. E.; Stephens, D. L.; Deems, R. A.; Li, S.; Asmus, K. M.; Woods, V. L., Jr.; Dennis, E. A. *J. Biol. Chem.* **2008**, *283*, 9820.
(45) Hamuro, Y.; Anand, G. S.; Kim, J. S.; Juliano, C.; Stranz, D. D.; Taylor, S. S.; Woods, V. L., Jr. *J. Mol. Biol.* **2004**, *340*, 1185.
(46) Jacobson, M. P.; Pincus, D. L.; Rapp, C. S.; Day, T. J. F.; Honig, B.; Shaw, D. E.; Friesner, R. A. *Proteins: Struct., Funct., Bioinf.* **2004**, *55*, 351.
(47) Rydel, T. J.; Williams, J. M.; Krieger, E.; Moshiri, F.; Stallings, W. C.; Brown, S. M.; Pershing, J. C.; Purcell, J. P.; Alibhai, M. F. *Biochemistry* **2003**, *42*, 6696.
(48) Humphrey, W.; Dalke, A.; Schulten, K. *J. Mol. Graphics Modell.* **1996**, *14*, 33.
(49) Phillips, J. C.; Braun, R.; Wang, W.; Gumbart, J.; Tajkhorshid, E.; Villa, E.; Chipot, C.; Skeel, R. D.; Kale, L.; Schulten, K. *J. Comput. Chem.* **2005**, *26*, 1781.
(50) MacKerell, A. D.; Banavali, N.; Foloppe, N. *Biopolymers* **2001**, *56*, 257.
(51) Ryckaert, J. P.; Ciccotti, G.; Berendsen, H. J. C. *J. Comput. Phys.* **1977**, *23*, 327.
(52) Adelman, S. A.; Doll, J. D. *J. Chem. Phys.* **1976**, *64*, 2375.
(53) Lin, J. H.; Perryman, A. L.; Schames, J. R.; McCammon, J. A. *J. Am. Chem. Soc.* **2002**, *124*, 5632.
(54) Friesner, R. A.; Banks, J. L.; Murphy, R. B.; Halgren, T. A.; Klicic, J. J.; Mainz, D. T.; Repasky, M. P.; Knoll, E. H.; Shelley, M.; Perry, J. K.; Shaw, D. E.; Francis, P.; Shenkin, P. S. *J. Med. Chem.* **2004**, *47*, 1739.
(55) Banks, J. L.; Beard, H. S.; Cao, Y. X.; Cho, A. E.; Damm, W.; Farid, R.; Felts, A. K.; Halgren, T. A.; Mainz, D. T.; Maple, J. R.; Murphy, R.; Philipp, D. M.; Repasky, M. P.; Zhang, L. Y.; Berne, B. J.; Friesner, R. A.; Gallicchio, E.; Levy, R. M. *J. Comput. Chem.* **2005**, *26*, 1752.
(56) CondeFrieboes, K.; Reynolds, L. J.; Lio, Y. C.; Hale, M. R.; Wasserman, H. H.; Dennis, E. A. *J. Am. Chem. Soc.* **1996**, *118*, 5519.